Computerized Medical Imaging and Graphics 118 (2024) 102464

Contents lists available at ScienceDirect

Computerized Medical Imaging and Graphics

journal homepage: www.elsevier.com/locate/compmedimag

Circumpapillary OCT-based multi-sector analysis of retinal layer thickness in patients with glaucoma and high myopia

Mateo Gende [a], Joaquim de Moura [a,*], Patricia Robles [b], Jose Fernández-Vigo [b], José M. Martínez-de-la-Casa [b], on behalf of GlaucoClub AI, Julián García-Feijóo [b], Jorge Novo [a], Marcos Ortega [a]

[a] Grupo VARPA, Instituto de Investigación Biomédica de A Coruña (INIBIC), Universidade da Coruña, Xubias de Arriba, 84, 15006 A Coruña, Spain
[b] Departamento de Oftalmología, Hospital Clínico San Carlos, Profesor Martín Lagos, s/n. Madrid, Spain

ARTICLE INFO

Keywords:
Glaucoma
Myopia
Deep learning
Segmentation
Computer-aided diagnosis
Ophthalmology

ABSTRACT

Glaucoma is the leading cause of irreversible blindness worldwide. The diagnosis process for glaucoma involves the measurement of the thickness of retinal layers in order to track its degeneration. The elongated shape of highly myopic eyes can hinder this diagnosis process, since it affects the OCT scanning process, producing deformations that can mimic or mask the degeneration caused by glaucoma. In this work, we present the first comprehensive cross-disease analysis that is focused on the anatomical structures most impacted in glaucoma and high myopia patients, facilitating precise differential diagnosis from those solely afflicted by myopia. To achieve this, a fully automatic approach for the retinal layer segmentation was specifically tailored for the accurate measurement of retinal thickness in both highly myopic and emmetropic eyes. To the best of our knowledge, this is the first approach proposed for the analysis of retinal layers in circumpapillary optical coherence tomography images that takes into account the elongation of the eyes in myopia, thus addressing critical diagnostic needs. The results from this study indicate that the temporal superior (mean difference 11.1 μm, $p < 0.05$), nasal inferior (13.1 μm, $p < 0.01$) and temporal inferior (13.3 μm, $p < 0.01$) sectors of the retinal nerve fibre layer show the most significant reduction in retinal thickness in patients of glaucoma and myopia with regards to patients of myopia.

1. Introduction

Glaucoma is currently considered the leading cause of irreversible blindness by the World Health Organization (W.H. Organization, 2019). In this neurodegenerative disease, damage to the optic nerve leads to the degeneration of the retinal layers responsible for the transmission of visual information to the brain. This degeneration is progressive, and begins affecting the peripheral vision, leading to it gradually affecting tissue before it is noticed. Since the effects of glaucoma cannot be reversed and only mitigated, an early diagnosis of glaucoma is paramount in preserving patient vision. However, the lack of symptoms during the onset of the disease, paired with the difficulty of assessing the tissue for progressive damage, leads to the significant under-diagnosis of this disease (Shaikh et al., 2014; Chua et al., 2015). This difficulty arises from different factors: first, the aforementioned lack of symptoms during early glaucoma may lead to patients not seeking attention on time; second, the challenge of detecting glaucoma by visual inspection of the eye fundus, since there is significant variation in the appearance of normal eyes; and third, the effects of other coexisting diseases, which may mask or alter the appearance of signs of glaucoma. Overall, the diagnosis process for glaucoma is a complicated one, lacking a singular test that can confirm its presence before it begins affecting the functional visual field and requiring a multi-pronged approach.

The course of glaucoma generally begins with damage to the optic nerve. In most cases, this damage is caused by an increase in pressure inside the eye, although other causes exist, such as in normal tension glaucoma. The damage to the optic nerve can manifest as a "cupping" of the optic disc (OD). By measuring the ratio between the optic cup and the OD, it is possible to establish an indication of whether there is a deformation of the optic nerve leading to glaucoma (Carpel and Engstrom, 1981). This cup-to-disc ratio has been used extensively for the automatic classification of glaucoma patients (Hervella et al., 2022; Jiang et al., 2020; Kumar et al., 2023).

* Corresponding author.
E-mail addresses: m.gende@udc.es (M. Gende), joaquim.demoura@udc.es (J. de Moura), p.robles.amor@gmail.com (P. Robles), jfvigo@hotmail.com (J. Fernández-Vigo), jmmartinezcasa@gmail.com (J.M. Martínez-de-la-Casa), julianga@ucm.es (J. García-Feijóo), jnovo@udc.es (J. Novo), mortega@udc.es (M. Ortega).

https://doi.org/10.1016/j.compmedimag.2024.102464
Received 19 June 2024; Received in revised form 10 October 2024; Accepted 3 November 2024
Available online 19 November 2024

However, other diseases such as myopia (Leung et al., 2007) can cause deformations to the OD which are unrelated to glaucomatous damage. This greatly complicates the diagnosis process for this disease. Myopia is characterised by an increase in axial length, which leads to far-away objects being out of focus. Several studies have shown that high myopia can be a risk factor for glaucoma (Czudowska et al., 2010; Marcus et al., 2011), with myopes being considered generally more likely to develop glaucoma. Moreover, the elongation of highly myopic eyes can pose a challenge for the diagnosis of glaucoma, since it can cause non-glaucomatous deformations on the optic nerve head which may hinder interpretability (Bikbov et al., 2020). This leads to an increased risk of misdiagnosing highly myopic eyes as glaucomatous (Yamashita et al., 2014; Leung et al., 2012). In this regard, the specific deformations caused by myopia can disrupt the regular diagnosis process for glaucoma in different ways: an increase in pallor in the neuroretinal rim makes it lose contrast against the optic cup which, along with the flattening of the cup and the stretching of the OD, makes the ophthalmoscopic observation of the optic nerve area unreliable for the diagnosis of glaucoma in myopic eyes (Kang et al., 2010; Tan et al., 2019).

The use of Optical Coherence Tomography (OCT) can provide structural information of the anatomy and conditions of the OD. This has established OCT as a fundamental tool in diagnosing and assessing glaucoma (Mwanza et al., 2012; Dong et al., 2016) as well as other ocular diseases such as macular oedema (Hu et al., 2019; Vidal et al., 2023), epiretinal membrane (Hirano et al., 2010; Ayhan et al., 2024), or age-related macular degeneration (Schlegl et al., 2018; Rispoli et al., 2023). OCT enables the direct observation of the retinal layers, with the Retinal Nerve Fibre Layer (RNFL) emerging as a valuable predictor for early glaucomatous changes (Leung et al., 2005, 2010), overcoming some of the limitations of OD assessment in myopic eyes (Kang et al., 2010). Nevertheless, the use of OCT for assessing myopic eyes for glaucomatous damage is not without its challenges. First, the shape of myopic eyes can differ greatly from that of emmetropic ones (Kim et al., 2009; Tabernero and Schaeffel, 2009; Moriyama et al., 2011; Murphy et al., 2017). This can complicate the assessment of a measured RNFL thickness against a normative database that does not take the particularities of myopic eyes into account. Second, the tilting at the base of the optic nerve caused by the elongation of the globe in myopic eyes can change the incidence of the scanning sweep of the OCT platform. This can make the scanned surface oblique instead of perpendicular to the scanning beam, changing the perceived distance of the sample and causing a distortion in the scan (Fig. 1). The effects of this distortion can range from a mild curvature in the imaged retinal surface to images where parts of the retina lie outside of the imaged area. Thus, more elongated eyes tend to introduce distortions that greatly hinder the diagnosis process. This is especially relevant for diseases such as glaucoma in which only gradual changes are apparent and may be hidden or changed by the distortion caused by myopia.

The advantages of OCT as an imaging technique for the early diagnosis of glaucoma drive the need for the development of automatic methods that can provide a robust measurement of the retinal layers. However, the aforementioned effects of high myopia in OCT scans pose a significant challenge in terms of both accuracy and repeatability. In this context, the effects of myopia on the assessment of glaucoma create one of the most adverse scenarios for both visual and computer-aided inspection. A challenging scenario that remains to be properly addressed by platform manufacturers, placing those patients who already are at a higher risk of developing glaucoma in a disadvantaged position for diagnosis, potentially leading to treatment delays and irreversible vision loss. Thus, the development of a methodology able to provide a precise and reproducible assessment of the condition of retinal layers holds significant value, serving not only as a diagnostic support tool for clinical experts but also as a means for clinical researchers to conduct studies which can contribute to understanding the effects of glaucoma and ultimately aid in the development of treatment strategies to preserve patient sight.

1.1. Related works

The advantages of OCT as an imaging technique for the early diagnosis of glaucoma, along with the specific challenges presented by the effects of myopia motivate the development of an automatic approach specifically adapted for the accurate measurement of the retinal layers in elongated eyes. While OCT imaging platform manufacturers have introduced software changes to address the morphology of myopic patients, these changes rarely result in an improvement in terms of the quality of acquired measurements (Holló et al., 2016; Suwan et al., 2018).

Due to its relevance for the diagnosis of glaucoma and other retinal and systemic diseases, several approaches have been proposed for the automatic segmentation of retinal layers. Roy et al. proposed the ReLayNet architecture (Roy et al., 2017), which used an encoder–decoder deep neural network structure to determine both the limits of the retinal layers as well as subretinal fluid. By employing a loss composed of Dice overlap and weighted logistic regression, this architecture achieved remarkable results in retinal layer segmentation. Berenguer-Vidal et al. (2021) presented two methods for retinal layer segmentation in circumpapillary OCT images. The first method used a deep learning architecture to segment the retinal layers, while the second method employed deformable models to adapt an initial estimation of the layer position to a final refined segmentation. Karn and Abdulla (2024) proposed a hybrid attention, U-Net based approach for the segmentation of three sets of retinal layers in macular images. Their results showed that by incorporating attention to the base architecture, the results could be improved. In the work by Cao et al. (2024) the authors incorporated self-attention into a convolutional neural network so that it can provide the missing contextual information needed in the convolutional operations.

Conversely, fewer computational approaches have been proposed for the assessment of glaucoma in OCT images taking myopic patients into account. Hsieh et al. (2020) presented a Fourier analysis of the thickness of the RNFL as a way to diagnose glaucoma in myopic eyes, relying on the automatic measurements produced by the imaging platform. Russakoff et al. (2020) proposed the use of a 3D system to predict whether patients should be referred for glaucoma using macular cubes. Their results showed a decrease of performance on severe myopia cases. More recently, Kim et al. (2023) presented a deep learning-based system with promising results for the diagnosis of glaucoma in myopic eyes using vertical macular cubes. Nevertheless, these past approaches show significant shortcomings when dealing with highly myopic eyes. Furthermore, all of these approaches are focused on the macular region of the eye. While this area of the eye is less affected by the elongation caused by myopia and can also show changes due to glaucoma, these changes are usually apparent in later stages of the disease, when the disease has already started causing irreversible vision loss. On the other hand, the circumpapillary area has been found to provide a higher discriminatory power in glaucoma (Na et al., 2011), with the recommended approach being a combined analysis of macular and circumpapillary features (Mwanza and Budenz, 2016; Na et al., 2013). However, an accurate segmentation of the retinal layers in the area surrounding the OD, the area where the myopic deformations are more severe, remains to be addressed.

1.2. Main contributions

In this work, we present a complete, multi-sector study of retinal layer thickness across cases of glaucoma and myopia. By comparing the thickness measurements among patients diagnosed with glaucoma and myopia, those solely with glaucoma, individuals exclusively with myopia, and a control group, the sectors most affected by glaucoma-related degeneration can be identified so that they can be used for differential diagnosis. In order to achieve a precise and accurate segmentation of the retinal layers in highly myopic eyes, we developed

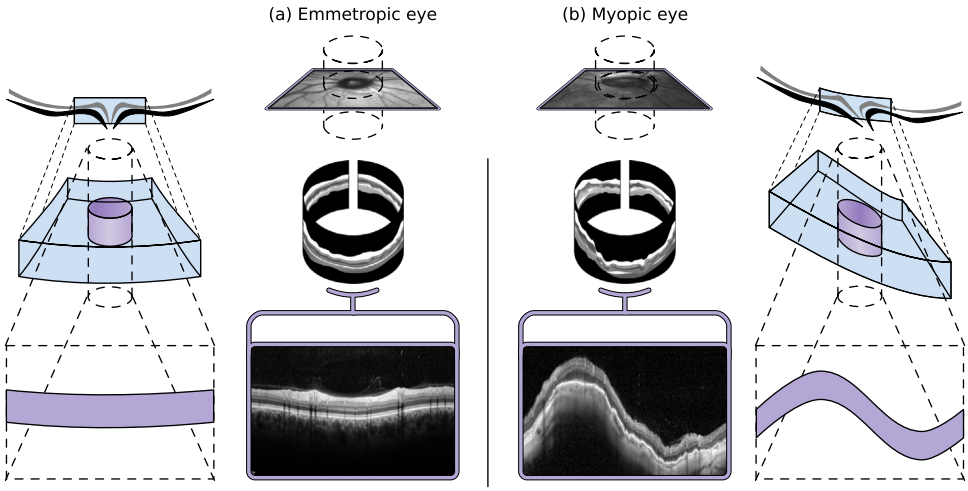

Fig. 1. Effects of axial elongation on the visualisations on OCT scans in the circumpapillary region. (a) In an emmetropic eye, the scanning direction is perpendicular to the tissue, producing a mostly flat scan. (b) In a myopic eye, the elongation can introduce a tilt in the OD area, making the scan direction oblique and producing a distorted image of the tissue.

a methodology for the automatic assessment of retinal layers in circumpapillary OCT images of both myopic and emmetropic eyes. This methodology consists of two primary stages. The first stage involves the use of a baseline deep learning segmentation architecture to acquire an initial measurement of the retinal layers. The second stage is dedicated to the continuity and curvature analysis of the retinal layers. In this stage, the retina is analysed to compensate for the effect of a tilted scanning direction in elongated eyes, produced an accurate measurement of the thickness of its layers. A summary of the structure of the methodology can be found in Fig. 2.

The main contributions of this work can be summarised as follows:

- We conducted a comprehensive, cross-disease study of the retinal layers most affected by glaucomatous degeneration in emmetropic and highly myopic eyes. In this study, we measured the retinal layer thickness across six different sectors around the OD using a dataset of over 800 OCT scans of patients of glaucoma and myopia, patients diagnosed with glaucoma, myopic patients and control cases.
- The comprehensive cross-disease study enables the cross-comparison of the thicknesses of the different regions in great detail, providing valuable insight on the anatomical differences that can be used to better assess the conditions of patients of these two relevant eye diseases. Isolating the regions primarily affected by glaucoma in myopic patients enhances the capacity to distinguish between individuals solely afflicted by myopia and those also affected by glaucoma. This improvement in discrimination facilitates a more accurate assessment of the conditions of the patients, and contributing to the preservation of their sight.
- To conduct this study, we developed a fully automatic methodology for the segmentation of the retinal layers in peripapillary OCT scans specifically designed around the needs of highly myopic patients. A series of deep learning models were trained and validated using a fully annotated dataset of 139 circumpapillary OCT scans from patients of glaucoma. Notably, this methodology demonstrates the capability to segment the retinal layers as well as automatically compensate for the effects of ocular elongation, providing a robust and repeatable assessment of the retina.
- To the best of our knowledge, this constitutes the first proposal for the automatic assessment of neuro-retinal layers in circumpapillary OCT images specifically tailored around the specifically challenging conditions of highly myopic eyes, enabling the use of retinal layer thickness as a biomarker for glaucoma in highly myopic as well as emmetropic eyes.

The structure of this manuscript is as follows: Section 2 presents the materials and methods that were employed during this study. The results are presented, along with the relevant discussion in Section 3. Finally, Section 4 presents the most relevant conclusions that were drawn from this work, along with future lines of research.

2. Materials and methods

To enhance the replicability of this work, this section provides a comprehensive overview of the data utilised for developing the proposed methodology. Additionally, it includes detailed explanations of the proposed methodology, the cross-disease study conducted, the evaluation metrics employed, and the software and hardware resources that were utilised.

2.1. Datasets

Two distinct datasets were employed specifically for the development of this work. The first dataset was used to train and adjust the layer segmentation methodology, while the second dataset was employed to conduct the comprehensive study across myopia and glaucoma. The images were acquired using a Heidelberg SPECTRALIS® optical imaging platform. All images were standardised to a resolution of 1024×992 pixels. All of the data employed in this work was acquired in accordance with the Declaration of Helsinki. None of the patients included in the first dataset were included in the second dataset.

2.1.1. Retinal layer segmentation dataset

The first dataset consists of 139 circular OCT scans extracted from 20 eyes of 10 different patients. These images were used to train and validate the baseline retinal layer segmentation architecture. As such, the contained images were fully annotated with the location of three anatomical regions of interest. Fig. 3 displays these regions of interest in detail.

- RNFL: This layer is formed by the bundle of neural fibres transmitting the visual information back to the brain via the optic nerve. The RNFL can be located between the vitreous and the Ganglion Cell Layer (GCL). It is one of the main anatomical structures associated with glaucomatous damage, with several studies highlighting its potential for glaucoma diagnosis (Hood et al., 2013).

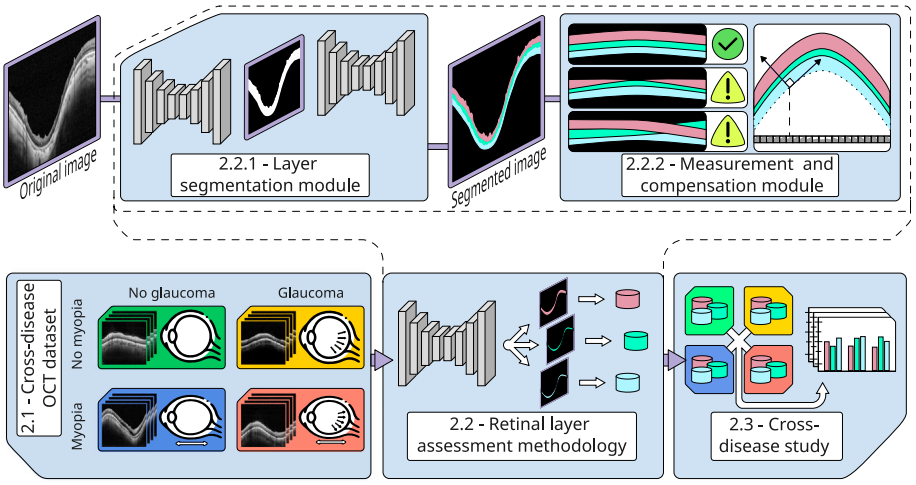

Fig. 2. Summary of the study herein presented. A two-stage retinal layer segmentation module is used to accurately measure the thickness of retinal layers while compensating for the deformations caused by myopia. This module is used to measure eyes from four different cohorts of glaucoma with myopia, glaucoma without myopia, myopia without glaucoma and control patients.

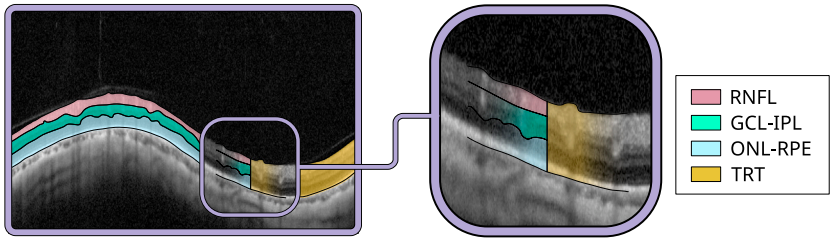

Fig. 3. Sample of the anatomical layers extracted by the proposed methodology.*RNFL*: Retinal Nerve Fibre Layer. *GCL-OPL*: Inner retina between the Ganglion Cell Layer and the Inner Plexiform Layer. *ONL-RPE*: Outer retina between the Outer Nuclear Layer and the Retinal Pigment Epithelium. *TRT*: Total retinal thickness, the set of all the segmented layers.

- Inner retina (GCL-OPL): This region comprises the anatomical structure responsible of transmitting the signal from the photoreceptors to the RNFL. This region is comprised of the GCL, the Inner and Outer Plexiform (OPL) layers. Different studies have linked the GCL-OPL region with changes related to glaucoma, to a lesser extent than the RNFL (Nouri-Mahdavi et al., 2013; Kotera et al., 2011).
- Outer retina (ONL-RPE): This region contains the photoreceptor cells responsible for detecting the changes in light intensity that are interpreted as vision. The outer retina contains the outer nuclear layer (ONL), the photoreceptors as well as the Retinal Pigment Epithelium (RPE). While not as heavily associated with glaucoma as the other two, this region also merits study since it contains the cells responsible for vision. Furthermore, the stable lower boundary between the RPE and the choroid is used as an indication of retinal curvature for measurement compensation.

2.1.2. Cross-disease dataset

The second dataset consists of a total of 809 circumpapillary OCT scans extracted from 474 eyes of 254 different patients. This dataset was employed to conduct the cross-disease study on the effects of glaucoma on the eyes of emmetropic and highly myopic eyes. These images are further subdivided into four classes according to the presence of glaucoma or myopia.

- Controls: This class contains patients without glaucoma or pathological myopia. It consists of patients clinically referred for refraction examination. The exclusion criteria employed were best corrected visual acuity lower than 0.5 with Snellen charts, along with a refractive error higher than 5 dioptre of spherical equivalent refraction or 3 dioptres of astigmatism or an intraocular pressure over 20mmHg. The related medical records were carefully reviewed for glaucoma, retinal pathology or the presence of prior episodes of optic neuritis. Patients presented an average age of 52 (95% CI [43, 61]), with female patients representing 68% of the total (95% CI [64.3%, 71.7%]). In total, 615 OCT scans belong to the Control class.
- Myopia: This class contains patients with pathological myopia but no glaucoma. These are patients with no clinical history of glaucoma and a refractive error higher than 6 dioptre spherical equivalent or an axial length greater than 26 mm. Patients presented an average age of 55 (95% CI [40, 60]), with female patients representing 52% of the total, and average myopia severity was measured at a -9.15 ± 2.57 dioptres. A total of 40 OCT scans are included in this class.
- Glaucoma: This class contains patients with diagnosed glaucoma but no pathological myopia, with a refractive error below 5 dioptre spherical equivalent and an axial length under 24 mm. Patients presented an average age of 76 (95% CI [73, 78]), with female patients representing 55% of the total (95% CI [37.0%, 72.6%]). In total, 100 OCT scans belong to this class.
- Glaucoma and myopia: Patients in this class have both a diagnosis of glaucoma as well as a refractive error higher than 6 dioptre or an axial length greater than 26 mm. Patients presented an average age of 66 (95% CI [63, 69]), with female patients representing 66% of the total (95% CI [53.6%, 78.6%]), and average myopia severity was measured at a -9.34 ± 4.26 dioptres. This class contains 54 OCT scans.

2.2. Retinal layer assessment methodology

In order to conduct the cross-disease segmentation study, an accurate measurement of the retinal layer thickness is required. To achieve

this, we developed a fully automatic, two-stage retinal layer assessment methodology which consists of two distinct stages. The first stage consists in the use of a robust retinal layer segmentation architecture that can provide an initial indication of the location of the retinal layers. This architecture provides a segmentation mask indicating the layer to which each pixel most likely belongs. This initial segmentation is then converted into an accurate measurement of retinal layer thickness during the second stage, which first validates whether the segmentation has been performed correctly in terms of layer continuity. If the image is deemed correctly segmented, the layer thickness is then measured across the retina, using the curvature of the segmentation masks as an estimation of the oblique direction in which the scan was acquired. This way, the curvature can be used to compensate the measurements and achieve a robust and accurate assessment of retinal layer thickness. Without this compensation stage, the measurements may be affected by the deformation caused by a tilted scan, which can obfuscate any relevant pathological changes leading to a poor assessment of the conditions of the retina.

2.2.1. Retinal layer segmentation module

The first stage of the methodology consists of a retinal layer segmentation module that can estimate the location of the retinal layers in the image. While several retinal layer segmentation architectures exist in the literature, MGU-net was selected for its robustness and its focus on the peripapillary region of the eye. This architecture was specifically developed for aiding in the diagnosis of glaucoma, with remarkable results when used for the segmentation of patients of glaucoma (Gende et al., 2023b) and other neurodegenerative diseases (Gende et al., 2023c,a). Moreover, this architecture has shown its ability to outperform other retinal layer segmentation approaches (Li et al., 2021).

This stage consists of two steps. In the first step, a module is used to separate the relevant retinal region from the background. This allows the removal of background noise as well as the propagation of the relevant visual features to the second step, which receives the original image masked using the output from the first step. This first stage allows the removal of the background and OD tissue from the segmentation, while enabling the further refinement in the second step. In this second step, the segmentation is further refined using a second module, separating each retinal layer into a different class and producing the final segmentation mask.

In order to make the best use of the available data, the model was first initialised to a pre-training performed on the dataset employed in its original publication (Li et al., 2021) using the parameters initially described therein. The model was then fine-tuned on peripapillary circular images from glaucoma patients. For more information regarding the dataset employed for model fine-tuning, please refer to Section 2.1.

Regarding training details, a 10-fold cross validation was followed at the patient level, using 80% of the images for training, 10% for validation and 10% for testing. The models were trained for a maximum of 50 epochs, using Cross-entropy and Dice loss. The optimisation was done using Adam (Kingma and Ba, 2015) with a learning rate of 1×10^{-3}, $\beta_1 = 0.9$ and $\beta_2 = 1\times10^{-4}$. 16 images were included per training batch. The validation loss was used as an indicator of the ability of the models to generalise to unseen images and avoid overfitting. To this end, a checkpoint of the model at the point with the lowest validation loss was employed for testing.

2.2.2. Measurement and compensation module

While the model in the first stage produces an accurate segmentation mask indicating the location of each retinal layer, a further refinement can ensure the quality of the segmentation and compensate for the effects of axial elongation. This stage can also be subdivided into two steps. In the first step, the continuity of the retinal layers is assessed as a way to detect and report errors, both in terms of image acquisition and image segmentation. In the second step, the curvature of the retinal scan is measured and used to compensate the retinal thickness measurement.

As previously stated, the deformations caused by the elongation of the eye can significantly impact the area that is imaged by OCT. In this regard, different situations can lead to images that either do not meet a minimum standards of quality to produce an accurate segmentation, or do not exclusively display the intended anatomical structures by imaging part of the OD or deviating significantly from it. For this reason, the continuity of the layers is used as an estimation of the segmentation quality. In this regard, images with continuous and consistent layers are deemed of sufficient quality, while the fraction of images where the layers break up or overlap whether due to poor image acquisition or errors by the segmentation model are flagged for re-acquisition or manual inspection. An example of this process can be found in Fig. 4. This not only helps detect errors caused by the segmentation architecture, but can also aid in the detection of other pathologies which affect the retinal layer structure, such as macular oedema, epiretinal membrane or retinal detachment.

By directly measuring the retinal thickness without taking into account the oblique direction in which the scans are taken in elongated eyes, the real thickness of the layers may be over-estimated. This over-estimation can lead to a delay in the diagnosis of glaucoma, since the effects of the increased axial length can mask the degenerative changes of this disease. Moreover, changes in the incidence of the scan may produce wildly varying measurements, which can be inconsistent along follow-up visits. In order to compensate for this tilted scanning direction and make the measurements as consistent as possible, a tilted-scan self-compensation method was devised based on the original baseline segmentation. This process uses the segmented boundary between the RPE and the choroid as an estimation of the position of the whole retina. Located in the outer parts of the retina, this boundary is less affected by vasculature and describes mostly a soft curve which can be used to characterise the whole curvature of the retina. Thus, within a segmentation mask, for every image column $n \in N$ there will be a pixel $y_n \in Y$ located over this boundary. Taking pixels $\{y_1, \dots, y_N\}$, one can extract the absolute derivative of the change in pixel height as a measurement of retinal curvature, with values closer to 0 indicating a flat retina and larger values indicating a slope. By differentiating at every column, an array of values $y'_n \in Y'$ can be constructed. Since the discrete nature of pixels can fail to capture the smooth slope of the retina, this array Y' is smoothed using a convolution operation with a flat structuring element with values $1/w$, where w is the width of the structuring element. Next, the vertical thickness of every retinal layer at every pixel column is measured and adapted according to Eq. (1).

$$H_{L,n} = (\max L(n) - \min L(n)) * \cos(\arctan(y'_n)) \tag{1}$$

where $L(n)$ is the set of pixels that belong to layer L in column n. This way, the slope is used to compensate from the overestimation of the layer thickness caused by measuring the curved retina (Fig. 5). Finally, the compensated measurements are filtered to remove any small deviations caused by the vascular structure of the eye using the same operation as for the slope Y'.

2.3. Cross-disease study

In order to better understand the separate effects of glaucoma and myopia on the observed retinal layer thickness, as well as to determine the areas that are most indicative of either disease, a comprehensive cross-disease study was conducted employing the previously described methodology. The aim of this study is to analyse potential anatomical differences that may characterise patients of glaucoma and myopia, helping improve both the diagnosis and assessment process of these pathologies. By characterising the changes that take place in the retina during the course of glaucoma, and contrasting them with the effects of myopia, the differential diagnosis process of these two diseases can be improved.

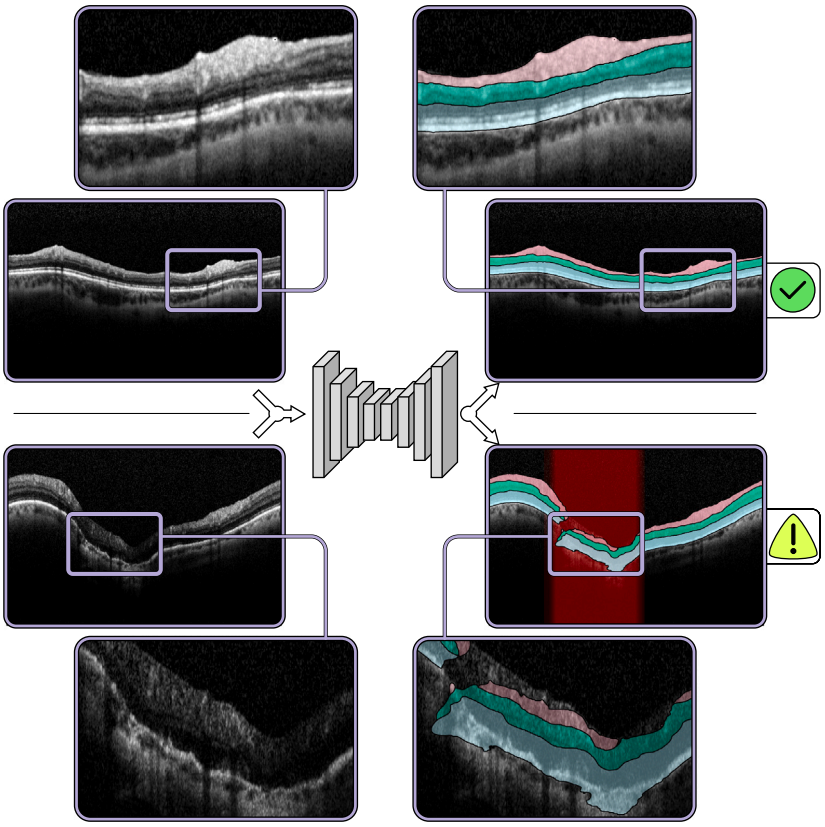

Fig. 4. Example of the error detection process showing a detailed view of the segmented area for ease of comparison. *Top*: segmentation of an image of sufficient quality showing a correct segmentation. *Bottom*: segmentation of an image with visibility problems affecting a specific area of an image (highlighted in red). While most of the image can be correctly segmented, the continuity problem caused by the deficient scan means that the measurements taken from this image can be unreliable, and the acquisition should be repeated.

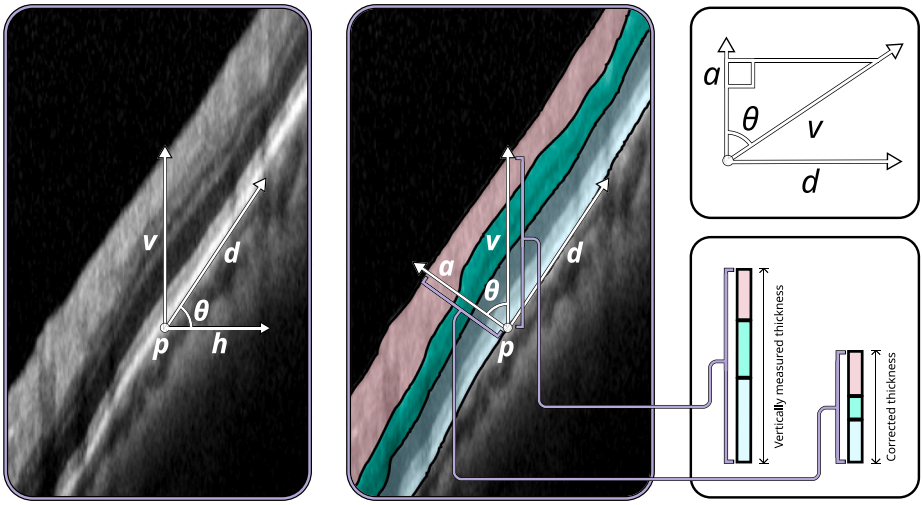

Fig. 5. Basic explanation of the angular tilt compensation employed to correct the measured thickness. At point p the angle θ is measured between the horizontal h and a line tangential to the RPE. A thickness measurement in the vertical direction v is taken and compensated using the cosine of θ to estimate the measurement in direction a perpendicular to the retinal surface. This way the estimated thickness at every point can be quickly and accurately estimated.

In this study, we compare the thickness of the different anatomical regions in patients of glaucoma and myopia, patients of glaucoma without pathological myopia, patients of pathological myopia without glaucoma, as well as control patients, thus covering all four possible combinations. First, the retinal layer thickness of the three anatomical regions that were considered is measured from the images using the proposed methodology. The thickness measurements are then subdivided according to the anatomical sector that they belong to. The distributions and angle spans for each sector can be found in Fig. 6. Then, the measurements are averaged within each sector, extracting a mean thickness value that summarises the sector thickness.

Three different analyses were undertaken in this study to explore the most prevalent and pertinent scenarios in glaucoma diagnosis. The initial analysis involved categorising patients only based on the presence or absence of glaucoma. Consequently, this analysis encompassed all cases indiscriminately, without specific consideration for the

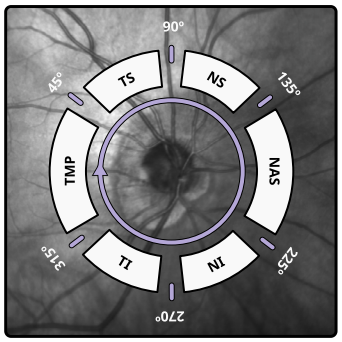

Sector		Angle span
TMP	Temporal	315° - 45°
TS	Temporal-Superior	45° - 90°
NS	Nasal-Superior	90° - 135°
NAS	Nasal	135° - 225°
NI	Nasal-Inferior	225° - 270°
TI	Temporal-Inferior	270° - 315°

Fig. 6. Location and angle spans of the anatomical sectors that were studied.

presence of high myopia among patients. The second analysis focused exclusively on myopic patients. By studying the differences between myopic patients with glaucoma, and those solely affected by myopia, it is posible to isolate the changes most likely caused by glaucomatous damage. In this sense, this analysis is the most likely to highlight the anatomical areas most affected by glaucomatous damage that have not been affected in patients who only have high myopia. Identification and characterisation of these areas can facilitate a more nuanced differential diagnosis for myopic patients. Finally, the patients with high myopia were excluded from the third analysis. Emmetropic patients still constitute the vast majority of cases that are referred for glaucoma. In this third analysis, the effects of glaucoma without myopia are studied in order to characterise the effects of glaucoma on most patients.

In all three analyses, the average thickness of each layer in every anatomical sector is grouped in classes according to their pathology and compared among each other. Significant differences between the retinal thicknesses of different groups can be indicative of pathology-related changes. By characterising when these changes are caused by glaucoma, it is possible to improve the differential diagnosis in highly myopic as well as emmetropic patients, contributing to an early assessment of glaucoma.

2.4. Evaluation

The following segmentation metrics were selected in order to exhaustively validate the automatic methodology:

$$Accuracy = \frac{TP+TN}{TP+TN+FP+FN} \tag{2}$$

$$Precision = \frac{TP}{TP+FP} \tag{3}$$

$$Recall = \frac{TP}{TP+FN} \tag{4}$$

$$Dice = \frac{2\times TP}{2\times TP+FP+FN} \tag{5}$$

TP, FP, TN and FN respectively denote True Positives, False Positives, True Negatives and False Negatives, measured at the pixel level. For statistical testing, due to the differences in variance and sample size, the unequal variances t-test (Welch, 1947); as defined in Eq. (6)

$$t = \frac{\bar{X}_1 - \bar{X}_2}{\sqrt{s^2_{\bar{X}_1} + s^2_{\bar{X}_2}}}, \tag{6}$$

where $\bar{X}_i$ denotes the group mean, $s_{\bar{X}_i} = \frac{s_i}{\sqrt{N_i}}$ denotes the standard error and N_i denotes sample size; was used to compare the anatomical regions in the comprehensive cross-disease test. Furthermore, three significance levels were considered at 95%, 99% and 99.9%, when comparing these test results.

Table 1
Test results for the segmentation models averaged across all 10 folds.

Region	Accuracy	Precision	Recall	Dice
RNFL	0.990 ± 0.005	0.897 ± 0.057	0.896 ± 0.071	0.895 ± 0.049
Inner Retina	0.991 ± 0.003	0.895 ± 0.049	0.905 ± 0.052	0.899 ± 0.042
Outer Retina	0.991 ± 0.005	0.950 ± 0.041	0.909 ± 0.070	0.928 ± 0.048
All regions	0.991 ± 0.004	0.914 ± 0.039	0.903 ± 0.057	0.907 ± 0.043

2.5. Software and hardware resources

The methodology was developed using the Python language (v.3.8.10). The models were trained and validated using the PyTorch library (version 1.12.1) (Paszke et al., 2019). Visual and numerical transformations were applied using the OpenCV library (version 4.5.5.62) and NumPy (version 1.21.4). All experiments were conducted using an NVIDIA A100 GPU, as well as an AMD EPYC 7763 64-Core CPU.

3. Results and discussion

The first part of this section is dedicated to the results of the automatic retinal layer segmentation methodology. The second part is focused on the comprehensive cross-disease study, including a comparison between all patients and a separate analysis within the myopic and the emmetropic patients.

3.1. Retinal layer segmentation module

The segmentation models were trained and tested following the process described in Section 2.2.1. Graphs for training and validation losses and dice scores can be found in Fig. 7, while the test results can be found in Table 1. With an overall Dice score of 0.91 ± 0.04, these results show that the automated models are able to accurately segment all three anatomical regions. These results are in line with those produced by other relevant and related retinal layer segmentation works (see Table 2). However, it should be noted that these results are those reported by each original publication and the lack of a publicly accessible circumpapillary OCT dataset of glaucoma patients precludes a fair comparison under the same conditions. Thus, the results presented in this table are those reported in each of the original publications and are not directly comparable. The model with the best test results in terms of Dice score was selected to perform the initial segmentation in the subsequent cross-disease study using the separate dataset.

3.2. Cross-disease study

The images from the second dataset were analysed using the best performing model from the previous stage. In order to better illustrate

Table 2
Comparison of the proposed retinal layer segmentation module with the results reported by other related retinal layer segmentation proposals. cpOCT denotes proposal was tested on circumpapillary OCT images. Glaucoma indicates proposal was tested on images from glaucomatous patients. Numbers indicate reported Dice score. A – denotes that the method in question does not report results on the relevant images or anatomical region.

	ReLayNet (Roy et al., 2017)	MGU-Net (Li et al., 2021)	Cao et al. (2024)	Karn and Abdulla (2024)	H-DLpNet (Berenguer-Vidal et al., 2021)	Proposed
cpOCT	–	–	–	–	✓	✓
Glaucoma	–	–	–	–	✓	✓
RNFL	0.90	0.83 ± 0.02	0.88	–	0.90 ± 0.03	0.90 ± 0.05
All regions	–	0.82 ± 0.02	0.87	0.81	–	0.91 ± 0.04

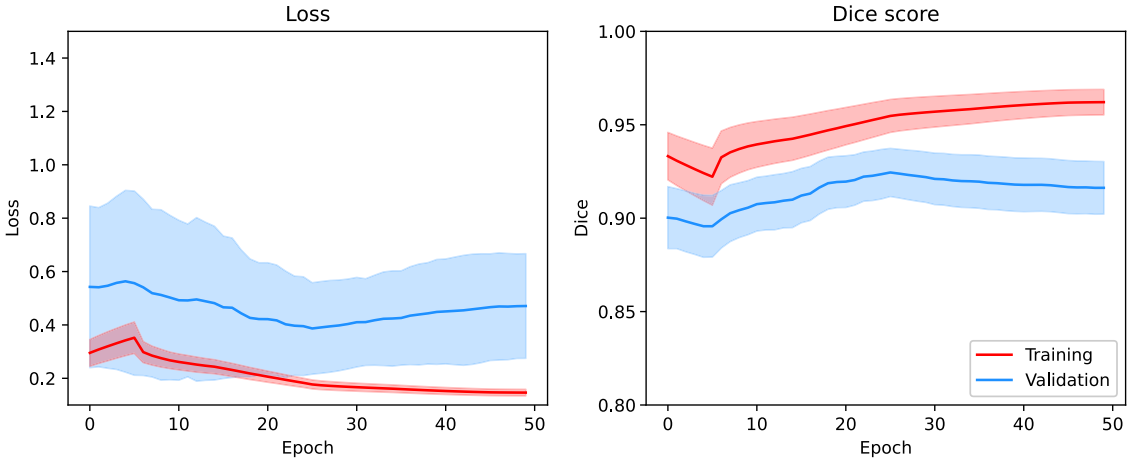

Fig. 7. Training and validation loss and Dice score for the segmentation models. Lines show the average, while shaded regions display the standard deviation for every epoch across all 10 folds.

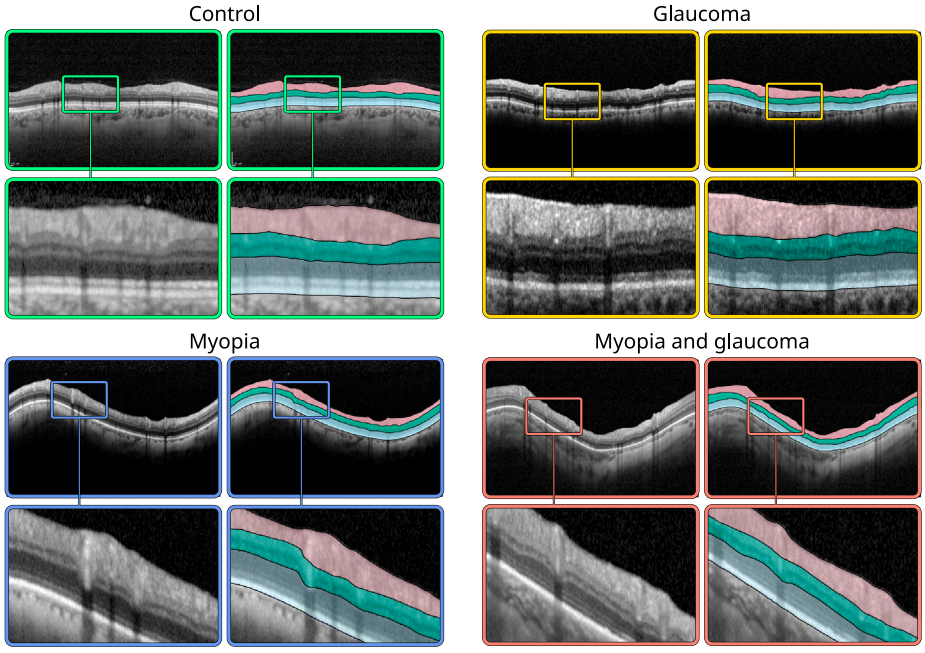

Fig. 8. Side by side comparison of segmentation samples produced by the model for the four classes.

the results and the anatomical differences caused by myopia and glaucoma, Fig. 8 displays some examples of the segmentations produced by this model for the four main classes. These images show that the model is able to accurately segment all three regions while adapting to the characteristic morphology of the patients of myopia.

A summary of the average thicknesses for each sector in each layer grouped by pathology can be found in Table 3. These results show that both glaucoma as well as myopia can cause a thinning of the retinal layers, but that these changes are not equal across the different sectors. First, the effects of glaucoma carry a more significant thinning of the RNFL in every sector but the NS and NAS, which are furthest away from the macula. High myopia, on the other hand, seems to have more effect in the GCL-OPL and ONL-RPE regions. For the emmetropic patients, who represent the majority of the population, the largest degenerative

Table 3
Average thickness for every anatomical region measured by the complete methodology. Values are shown in μm, separated by sector and grouped by pathology.

Group	Layer	TMP	TS	NS	NAS	NI	TI
Glaucoma and myopia	RNFL	45.2 ± 11.1	55.0 ± 20.9	46.9 ± 13.6	39.4 ± 9.0	44.3 ± 10.6	61.6 ± 19.3
	GCL-OPL	55.4 ± 8.9	42.6 ± 6.1	41.9 ± 6.5	43.0 ± 5.4	40.9 ± 5.8	43.5 ± 6.9
	ONL-RPE	68.7 ± 16.1	65.3 ± 19.6	67.3 ± 13.6	66.4 ± 12.7	62.9 ± 15.0	66.8 ± 23.6
Glaucoma and no myopia	RNFL	41.8 ± 9.8	56.1 ± 17.5	50.4 ± 16.8	43.3 ± 11.1	51.7 ± 18.5	57.5 ± 16.3
	GCL-OPL	61.3 ± 8.4	50.4 ± 7.9	47.9 ± 6.8	48.4 ± 5.1	45.0 ± 6.5	49.3 ± 7.9
	ONL-RPE	77.2 ± 10.0	71.7 ± 9.7	71.1 ± 8.9	72.2 ± 6.4	66.9 ± 7.7	69.1 ± 8.9
Myopia and no glaucoma	RNFL	47.7 ± 7.4	66.1 ± 22.1	49.7 ± 17.0	43.6 ± 11.2	57.4 ± 19.1	74.9 ± 18.1
	GCL-OPL	55.6 ± 10.1	43.9 ± 6.3	42.5 ± 7.7	42.2 ± 6.8	41.4 ± 5.7	43.8 ± 6.9
	ONL-RPE	63.4 ± 12.3	65.1 ± 16.8	63.2 ± 9.6	63.5 ± 12.1	63.5 ± 14.3	61.2 ± 12.4
Control	RNFL	54.8 ± 11.2	85.0 ± 17.7	75.4 ± 19.6	58.0 ± 9.8	80.1 ± 21.1	86.7 ± 18.9
	GCL-OPL	63.3 ± 11.8	49.1 ± 8.0	47.3 ± 7.2	52.9 ± 8.9	46.5 ± 7.5	48.1 ± 7.8
	ONL-RPE	75.8 ± 8.8	70.5 ± 10.1	70.5 ± 9.9	75.2 ± 7.4	68.9 ± 9.4	68.5 ± 8.6

Table 4
Average thickness as measured without using the tilted scan compensation. Values are shown in μm, separated by sector and grouped by pathology.

Group	Layer	TMP	TS	NS	NAS	NI	TI
Glaucoma and myopia	RNFL	63.7 ± 14.9	91.1 ± 31.9	80.7 ± 28.6	66.7 ± 17.2	82.7 ± 30.1	94.4 ± 30.7
	GCL-OPL	93.2 ± 13.6	76.8 ± 8.7	72.9 ± 8.7	73.5 ± 6.2	72.0 ± 7.6	75.1 ± 8.7
	ONL-RPE	127.2 ± 36.4	124.4 ± 44.0	121.9 ± 31.8	120.7 ± 25.6	122.5 ± 37.0	126.6 ± 46.9
Glaucoma and no myopia	RNFL	62.2 ± 18.2	87.0 ± 31.7	79.5 ± 28.4	66.1 ± 18.1	82.0 ± 29.7	87.8 ± 32.8
	GCL-OPL	99.1 ± 11.5	84.8 ± 9.8	81.5 ± 9.0	78.8 ± 6.9	76.8 ± 8.3	82.6 ± 9.2
	ONL-RPE	127.0 ± 18.7	121.5 ± 10.5	121.1 ± 9.8	118.2 ± 8.2	115.0 ± 8.8	116.7 ± 9.8
Myopia and no glaucoma	RNFL	53.1 ± 14.8	78.9 ± 27.8	72.8 ± 21.6	64.0 ± 19.6	76.4 ± 28.8	79.2 ± 34.5
	GCL-OPL	96.2 ± 16.8	77.2 ± 7.9	75.9 ± 6.9	73.9 ± 5.8	71.5 ± 7.3	80.1 ± 12.2
	ONL-RPE	120.1 ± 26.8	121.5 ± 29.3	119.2 ± 15.8	119.3 ± 17.3	118.9 ± 27.8	123.2 ± 34.0
Control	RNFL	55.0 ± 11.9	85.1 ± 18.4	75.7 ± 19.9	58.2 ± 10.2	80.0 ± 21.3	86.7 ± 19.1
	GCL-OPL	101.8 ± 17.7	82.5 ± 9.0	80.8 ± 6.9	85.6 ± 12.5	78.6 ± 7.4	80.9 ± 8.5
	ONL-RPE	122.8 ± 11.4	119.8 ± 15.6	121.5 ± 12.5	122.8 ± 10.9	118.5 ± 15.3	117.0 ± 17.6

effects can be found in the RNFL, with a larger reduction in the TS, NI and TI sectors. The NAS sector also shows a significant thickness decrease for all three anatomical regions as well as the TRT. This decrease is also significant in the NI sector, although to a lesser degree.

3.2.1. Tilted scan compensation

As a way to illustrate the relevance of the curvature compensation module, Table 4 represents the average thickness measured for each layer without employing this module. When compared to the results displayed in Table 3, it is clear that most patients affected with glaucoma and myopia appear to have a higher thickness than patients unaffected by these diseases in the layers most commonly affected by glaucomatous degeneration in the literature. Moreover, the use of this compensation module also helps reduce the variability between the images, since these deformations can change the automatically measured thicknesses along the axis of the image. This can be seen in the increase in standard deviation in Table 4 with respect to the values shown in Table 3.

3.2.2. Analysis across all cases

For the first comparison, the patients were grouped in two sets, according to whether they present signs of glaucoma or not. Thus, both groups contain patients with and without myopia, so that the main differences caused by glaucoma regardless of eye elongation can be highlighted. Fig. 9 displays a comparison of the average retinal thickness for each layer and each sector. Statistically significant differences between patients of glaucoma and controls were found for every sector in every layer. As could be seen from the results shown in Table 3, these differences seem more pronounced in the RNFL, the layer most directly associated with glaucomatous degeneration. On the other hand, the degeneration also seems to affect both the GCL-OPL and ONL-RPE regions, although the differences are proportionally smaller.

3.2.3. Analysis of myopic patients

By restricting the study to only the patients of myopia, the differences between glaucoma and control patients are less pronounced (Fig. 10). This is to be expected, since highly myopic eyes present a more varied morphology than emmetropic ones, as confirmed by previous research (Tabernero and Schaeffel, 2009; Moriyama et al., 2011). For these patients, no statistically significant differences were found for the GCL-OPL and ONL-RPE regions. Nonetheless, statistically significant differences were found in the RNFL layer. As previously mentioned, this layer is the most commonly associated with changes due to glaucoma. Significant differences were found for the TS (11.1 μm mean difference, $p = 0.0401$), NI (13.1 μm, $p = 0.0015$) and TI (13.3 μm, $p = 0.0048$) sectors.

As previously mentioned, myopic patients are at a comparatively greater risk of developing glaucoma, while the elongated shape of their eyes hindering diagnosis by affecting the measured retinal thickness. Using the proposed methodology specifically tailored for these patients, we were able to find significant differences in the TS, NI and TI sectors of the RNFL. These areas may merit further study for the differential diagnosis of glaucoma in the eyes of highly myopic patients.

Moreover, these results highlight the significance of the measurement and compensation module incorporated into the methodology. As illustrated in Fig. 8, OCT scans from highly myopic eyes exhibit a sinusoidal wave pattern, which can lead to overestimation of measurements in tilted regions critical for discrimination. The sectors that typically show the highest inclination in these tilted OCT scans are the TS, NS, TI and NI. By providing accurate measurements of retinal thickness in these sectors, the separability between patients who develop glaucoma and those solely affected by myopia becomes much clearer. This, in turn, not only enhances diagnostic accuracy but also improves the assessment of glaucoma progression.

3.2.4. Analysis of emmetropic patients

Finally, considering only the emmetropic patients, we can see that there are thickness reductions in the NAS and NI sectors for all three

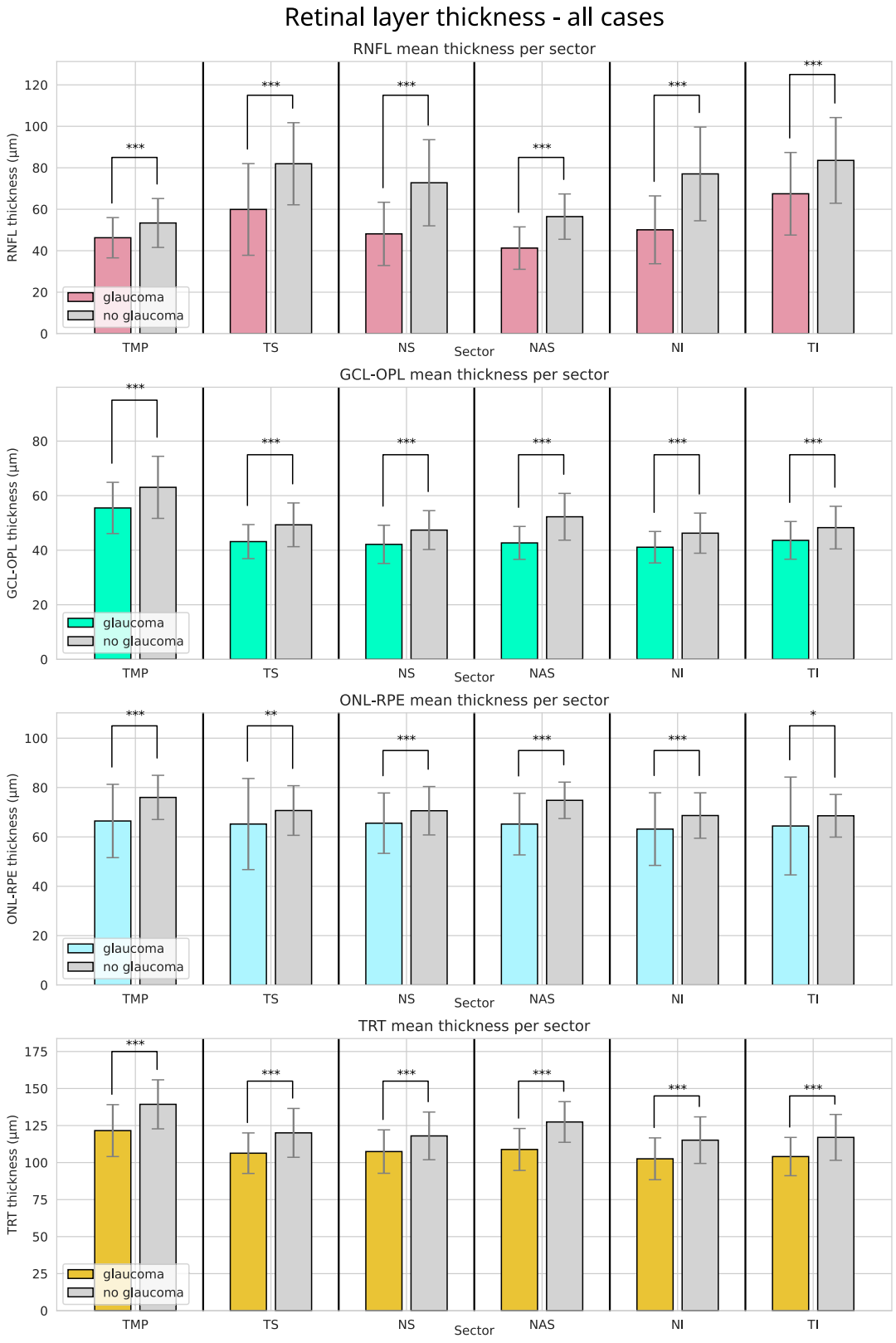

Fig. 9. Comparison of the average retinal thickness for all patients. Error bars show standard deviation. Brackets denote a statistically significant difference between the average thickness of glaucoma and control patients. *: $p < 0.05$, **: $p < 0.01$, ***: $p < 0.001$.

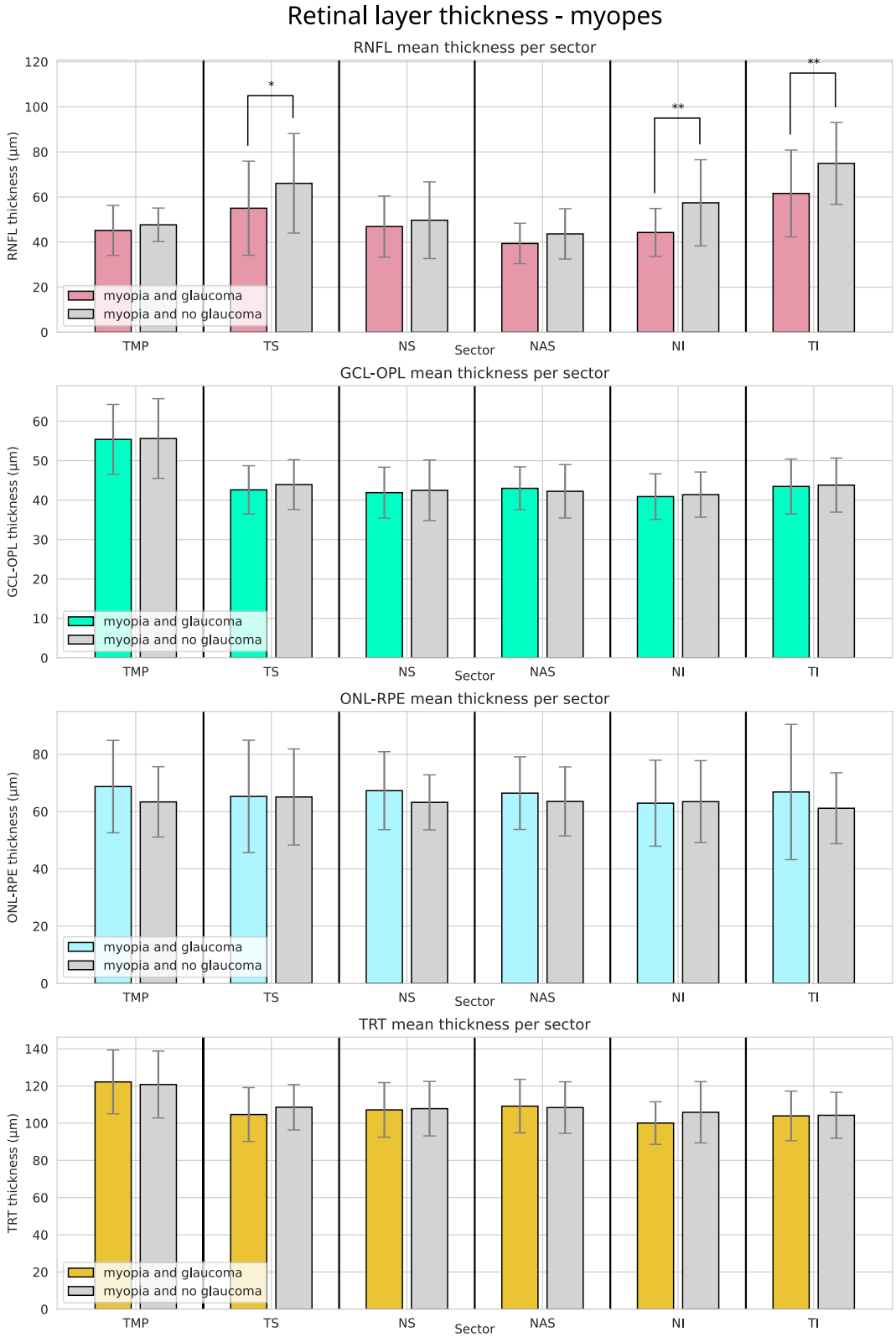

Fig. 10. Comparison of the average retinal thickness for the patients of glaucoma and myopia. Error bars show standard deviation. Brackets denote a statistically significant difference between the average thickness of glaucoma and control patients. *: $p < 0.05$, **: $p < 0.01$.

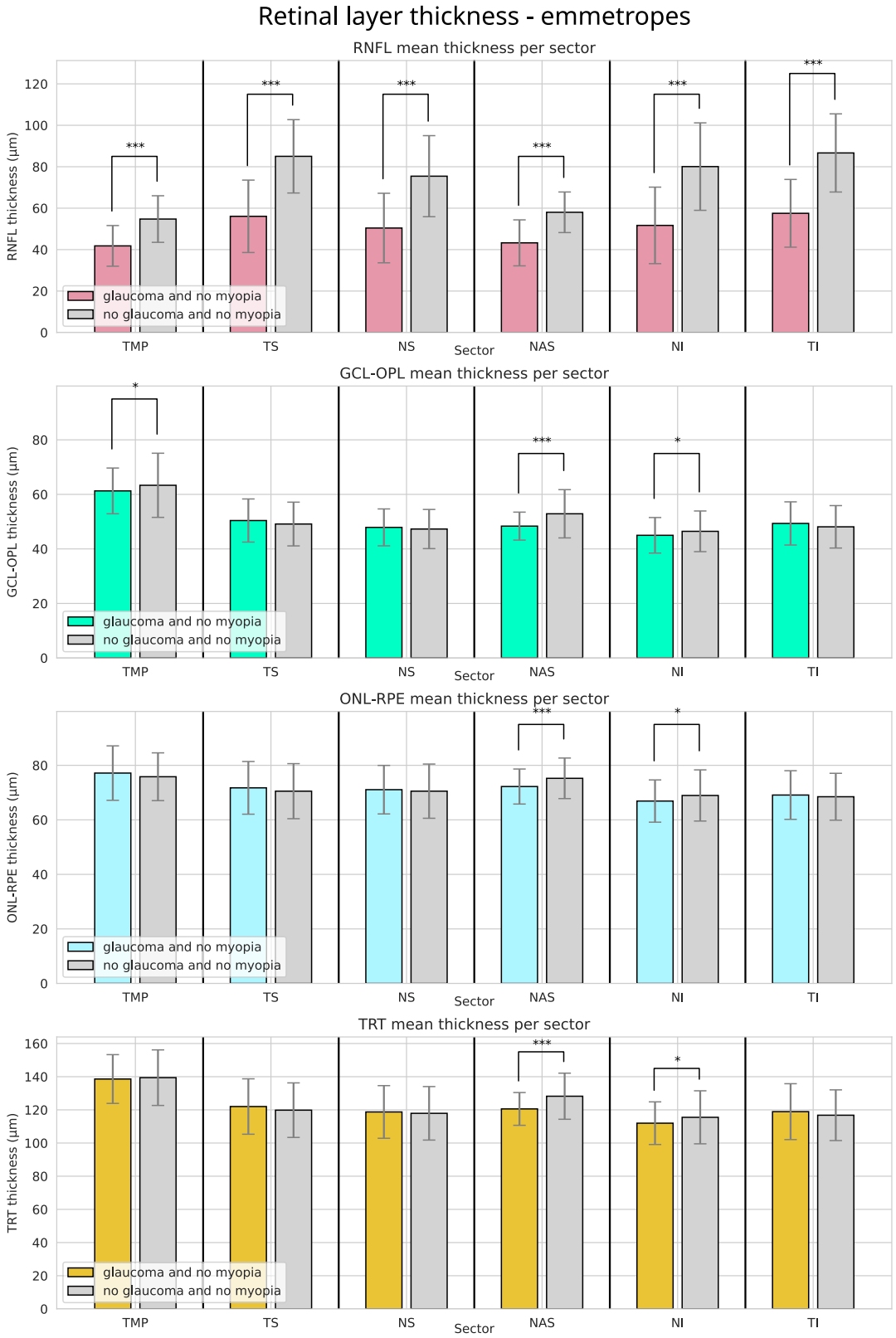

Fig. 11. Comparison of the average retinal thickness for the patients of glaucoma excluding myopes. Error bars show standard deviation. Brackets denote a statistically significant difference between the average thickness of glaucoma and control patients. *: $p < 0.05$, **: $p < 0.01$, ***: $p < 0.001$.

anatomical regions, as well as a significant decrease in RNFL thickness (Fig. 11). The largest mean differences within the RNFL were found for the TS (28.9 μm, $p = 6 \times 10^{-23}$), NI (28.4 μm, $p = 4 \times 10^{-21}$) and TI (29.2 μm, $p = 4 \times 10^{-25}$) sectors.

In general terms, the TS, NI and TI sectors of the RNFL seem to provide the greatest discriminative power for glaucoma, with and without taking into account the deformations caused by myopia. By compensating for the effects of these deformations, it is possible to accurately assess the current state of the patients, enabling a precise tracking of the evolution of the retinal layers and providing a way to differentially diagnose patients of myopia and glaucoma without running the risk of over-estimating the current retinal layer thickness. Overall, the proposed methodology provides a robust and repeatable assessment of the retinal layers of the patients. This assessment enables accurate monitoring of changes during clinical follow-ups, facilitating improved tracking of patient conditions. Additionally, it supports early diagnosis of patients at elevated risk of glaucoma resulting from myopia.

4. Conclusions

OCT imaging is routinely used to diagnose and assess the state of glaucoma patients. By tracking the retinal layer thickness across consecutive followups, it is possible to measure the progressive degeneration caused by this disease. Highly myopic patients are at an increased risk of suffering from glaucoma. Furthermore, the deformations caused by the elongation of the eyes can mimic or mask the degenerative effects of this pathology, a problem that complicates the diagnosis process and remains to be properly addressed by platform manufacturers as well as most computer-aided diagnosis systems. In this work, we have presented a comprehensive, cross-disease study on the effects of glaucoma, measuring the thickness of each anatomical region (RNFL, GCL-OPL and ONL-RPE) within each sector of the perimetry of the optic disc in patients of glaucoma and myopia. Specifically, three distinct analyses were conducted. The first compared the degenerative effects of glaucoma in patients without consideration for myopia. The second focused exclusively on myopic patients, assessing the effects of glaucoma within this subgroup. Lastly, the third analysis excluded myopic patients altogether, allowing for a comparison of glaucomatous effects in non-myopic individuals. In order to undertake this study, we developed a fully automatic methodology for the segmentation of retinal layers in circumpapillary OCT images, specifically tailored to address the effects of myopia and aid in the diagnosis of glaucoma. This approach automatically segments the relevant anatomical regions as well as corrects the distorted measurements caused by the elongation of the eye in oblique OCT scans.

Overall, the results from the study show that statistically significant differences in retinal thickness can be found using this methodology when considering both emmetropic and myopic patients. Furthermore, this study shows that the areas affected by glaucoma and high myopia are different, both in terms of the retinal layers and of the affected sectors. A significant reduction in retinal layer thickness was found for all patients when discriminating by glaucoma. Within the myopic patients, whose characteristic eye morphology complicates getting accurate measurements, we were able to find significant differences in RNFL thickness in the TS, NI and TI sectors.

To the best of our knowledge, this constitutes the first approach specifically designed for the retinal layer assessment of circular peripapillary OCT scans in highly myopic patients in the literature. A particularly challenging scenario, as most existing general-purpose approaches fail to accurately assess retinal layers in highly myopic eyes due to the significant deformations and elongations present. Our methodology simplifies the differential diagnosis process of glaucoma for highly myopic patients, enabling early treatment and helping preserve patient sight.

In the future, this methodology could be extended to other retinal diseases which could be affected by myopia, or to consider a more detailed analysis of the anatomical layers, such as a separate study of the GCL which has also been found to be associated to glaucomatous damage in the literature. Future approaches may include the study different automatic diagnosis approaches using the compensated measurements over the retinal layers. Moreover, the methodology proposed in this work could be incorporated into an complete pipeline aimed at the automatic diagnosis of glaucoma in emmetropic and myopic patients. By characterising which retinal layers and regions are most likely damaged by glaucoma, and which are affected by myopia could further simplify the diagnosis process of this relevant disease for the patients who are at a greater risk of contracting it and being misdiagnosed.

CRediT authorship contribution statement

Mateo Gende: Writing – original draft, Visualization, Software, Methodology. **Joaquim de Moura:** Writing – review & editing, Supervision, Resources, Project administration, Funding acquisition, Conceptualization. **Patricia Robles:** Writing – review & editing, Resources, Data curation. **Jose Fernández-Vigo:** Writing – review & editing, Validation, Supervision, Resources. **José M. Martínez-de-la-Casa:** Writing – review & editing, Validation, Supervision, Resources. **Julián García-Feijóo:** Writing – review & editing, Validation, Supervision, Resources. **Jorge Novo:** Writing – review & editing, Supervision, Resources, Project administration, Funding acquisition, Conceptualization. **Marcos Ortega:** Writing – review & editing, Supervision, Resources, Project administration, Conceptualization.

Declaration of competing interest

The authors declare that they have no known competing financial interests or personal relationships that could have appeared to influence the work reported in this paper.

Acknowledgements

This research was funded by Ministerio de Ciencia e Innovación, Government of Spain [research projects PDC2022-133132-I00, TED2021-131201B-I00, and PID2023-148913OB-I00]; Consellería de Cultura, Educación e Universidade, Xunta de Galicia, through Grupos de Referencia Competitiva [grant number ED431C 2024/33], predoctoral grant [grant number ED481A 2021/161]. This work was supported by the Instituto de Salud Carlos III (ISCIII) under the grant [FORT23/00010] as part of the Programa FORTALECE of Ministerio de Ciencia e Innovación and research project [PI23/00828]: Desarrollo *y* evaluación de un algoritmo de detección de glaucoma a partir de un abordaje multimodal en pacientes con miopía magna, as well as Thea Research Grant 2022-2024. The funding organisations had no role in the design or conduct of this research. Funding for open access charge: Universidade da Coruña/CISUG.

Data availability

Data will be made available on request.

References

Ayhan, M.S., Neubauer, J., Uzel, M.M., Gelisken, F., Berens, P., 2024. Interpretable detection of epiretinal membrane from optical coherence tomography with deep neural networks. Sci. Rep. 14 (1), http://dx.doi.org/10.1038/s41598-024-57798-1.

Berenguer-Vidal, R., Verdú-Monedero, R., Morales-Sánchez, J., Sellés-Navarro, I., del Amor, R., García, G., Naranjo, V., 2021. Automatic segmentation of the retinal nerve fiber layer by means of mathematical morphology and deformable models in 2D optical coherence tomography imaging. Sensors 21 (23), 8027. http://dx.doi.org/10.3390/s21238027.

Bikbov, M.M., Gilmanshin, T.R., Kazakbaeva, G.M., Zainullin, R.M., Rakhimova, E.M., Rusakova, I.A., Bolshakova, N.I., Safiullina, K.R., Zaynetdinov, A.F., Zinatullin, A.A., Nuriev, I.F., Khalimov, T.A., Panda-Jonas, S., Arslangareeva, I.I., Bikbova, G.M., Yakupova, D.F., Uzianbaeva, Y.V., Jonas, J.B., 2020. Prevalence of myopic maculopathy among adults in a Russian population. JAMA Network Open 3 (3), e200567. http://dx.doi.org/10.1001/jamanetworkopen.2020.0567.

Cao, G., Wu, Y., Peng, Z., Zhou, Z., Dai, C., 2024. Self-attention CNN for retinal layer segmentation in OCT. Biomed. Opt. Express 15 (3), 1605. http://dx.doi.org/10.1364/boe.510464.

Carpel, E.F., Engstrom, P.F., 1981. The normal cup-disk ratio. Am. J. Ophthalmol. 91 (5), 588–597. http://dx.doi.org/10.1016/0002-9394(81)90056-8.

Chua, J., Baskaran, M., Ong, P.G., Zheng, Y., Wong, T.Y., Aung, T., Cheng, C.-Y., 2015. Prevalence, risk factors, and visual features of undiagnosed glaucoma: The Singapore epidemiology of eye diseases study. JAMA Ophthalmol. 133 (8), 938. http://dx.doi.org/10.1001/jamaophthalmol.2015.1478.

Czudowska, M.A., Ramdas, W.D., Wolfs, R.C., Hofman, A., De Jong, P.T., Vingerling, J.R., Jansonius, N.M., 2010. Incidence of glaucomatous visual field loss: A ten-year follow-up from the rotterdam study. Ophthalmology 117 (9), 1705–1712. http://dx.doi.org/10.1016/j.ophtha.2010.01.034.

Dong, Z.M., Wollstein, G., Schuman, J.S., 2016. Clinical utility of optical coherence tomography in Glaucoma. Invest. Opthalmol. Vis. Sci. 57 (9), OCT556. http://dx.doi.org/10.1167/iovs.16-19933.

Gende, M., de Moura, J., Cordón, B., Vilades, E., García-Martín, E., Sánchez, C.I., Novo, J., Ortega, M., 2023a. Automatic deep learning-based models for retinal layer thickness analysis as a biomarker for neurodegenerative diseases. Invest. Ophthalmol. Vis. Sci. 64 (8), 1122–1122.

Gende, M., de Moura, J., Fernández-Vigo, J.I., Martínez-de-la Casa, J.M., García-Feijóo, J., Novo, J., Ortega, M., 2023b. Robust multi-view approaches for retinal layer segmentation in glaucoma patients via transfer learning. Quant. Imag. Med. Surgery 13 (5), 2846–2859. http://dx.doi.org/10.21037/qims-22-959.

Gende, M., Mallen, V., de Moura, J., Cordón, B., Garcia-Martin, E., Sánchez, C.I., Novo, J., Ortega, M., 2023c. Automatic segmentation of retinal layers in multiple neurodegenerative disorder scenarios. IEEE J. Biomed. Health Inf. 27 (11), 5483–5494. http://dx.doi.org/10.1109/JBHI.2023.3313392.

Hervella, Á.S., Rouco, J., Novo, J., Ortega, M., 2022. End-to-end multi-task learning for simultaneous optic disc and cup segmentation and glaucoma classification in eye fundus images. Appl. Soft Comput. 116, 108347. http://dx.doi.org/10.1016/j.asoc.2021.108347.

Hirano, Y., Yasukawa, Ogura, Y., 2010. Optical coherence tomography guided peeling of macular epiretinal membrane. Clin. Ophthalmol. 27. http://dx.doi.org/10.2147/opth.s16031.

Holló, G., Shu-wei, H., Naghizadeh, F., 2016. Evaluation of a new software version of the RTVue optical coherence tomograph for image segmentation and detection of glaucoma in high myopia. J. Glaucoma 25 (6), e615–e619. http://dx.doi.org/10.1097/ijg.0000000000000290.

Hood, D.C., Raza, A.S., de Moraes, C.G.V., Liebmann, J.M., Ritch, R., 2013. Glaucomatous damage of the macula. Progr. Ret. Eye Res. 32, 1–21. http://dx.doi.org/10.1016/j.preteyeres.2012.08.003.

Hsieh, M.-H., Chang, Y.-F., Liu, C.J.-L., Ko, Y.-C., 2020. Fourier analysis of circumpapillary retinal nerve fiber layer thickness in optical coherence tomography for differentiating myopia and glaucoma. Sci. Rep. 10 (1), http://dx.doi.org/10.1038/s41598-020-67334-6.

Hu, J., Chen, Y., Yi, Z., 2019. Automated segmentation of macular edema in OCT using deep neural networks. Med. Image Anal. 55, 216–227. http://dx.doi.org/10.1016/j.media.2019.05.002.

Jiang, Y., Duan, L., Cheng, J., Gu, Z., Xia, H., Fu, H., Li, C., Liu, J., 2020. JointRCNN: A region-based convolutional neural network for optic disc and cup segmentation. IEEE Trans. Biomed. Eng. 67 (2), 335–343. http://dx.doi.org/10.1109/tbme.2019.2913211.

Kang, S.H., Hong, S.W., Im, S.K., Lee, S.H., Ahn, M.D., 2010. Effect of myopia on the thickness of the retinal nerve fiber layer measured by cirrus HD optical coherence tomography. Invest. Opthalmol. Vis. Sci. 51 (8), 4075. http://dx.doi.org/10.1167/iovs.09-4737.

Karn, P.K., Abdulla, W.H., 2024. Advancing ocular imaging: A hybrid attention mechanism-based U-net model for precise segmentation of sub-retinal layers in OCT images. Bioengineering 11 (3), 240. http://dx.doi.org/10.3390/bioengineering11030240.

Kim, M.J., Lee, E.J., Kim, T.-W., 2009. Peripapillary retinal nerve fibre layer thickness profile in subjects with myopia measured using the stratus optical coherence tomography. Br. J. Ophthalmol. 94 (1), 115–120. http://dx.doi.org/10.1136/bjo.2009.162206.

Kim, J.-A., Yoon, H., Lee, D., Kim, M., Choi, J., Lee, E.J., Kim, T.-W., 2023. Development of a deep learning system to detect glaucoma using macular vertical optical coherence tomography scans of myopic eyes. Sci. Rep. 13 (1), http://dx.doi.org/10.1038/s41598-023-34794-5.

Kingma, D.P., Ba, J., 2015. Adam: A method for stochastic optimization. In: Bengio, Y., LeCun, Y. (Eds.), 3rd International Conference on Learning Representations, ICLR 2015, San Diego, CA, USA, May 7-9, 2015, Conference Track Proceedings. URL http://arxiv.org/abs/1412.6980.

Kotera, Y., Hangai, M., Hirose, F., Mori, S., Yoshimura, N., 2011. Three-dimensional imaging of macular inner structures in glaucoma by using spectral-domain optical coherence tomography. Invest. Opthal. Vis. Sci. 52 (3), 1412. http://dx.doi.org/10.1167/iovs.10-5572.

Kumar, V.V.N.S., Harinath Reddy, G., GiriPrasad, M., 2023. A novel glaucoma detection model using unet++-based segmentation and ResNet with GRU-based optimized deep learning. Biomed. Signal Process. Control 86, 105069. http://dx.doi.org/10.1016/j.bspc.2023.105069.

Leung, C.K., Chan, W.-M., Yung, W.-H., Ng, A.C., Woo, J., Tsang, M.-K., Tse, R.K., 2005. Comparison of macular and peripapillary measurements for the detection of glaucoma. Ophthalmology 112 (3), 391–400. http://dx.doi.org/10.1016/j.ophtha.2004.10.020.

Leung, C.K.-s., Cheng, A.C.K., Chong, K.K.L., Leung, K.S., Mohamed, S., Lau, C.S.L., Cheung, C.Y.L., Chu, G.C.-h., Lai, R.Y.K., Pang, C.C.P., Lam, D.S.C., 2007. Optic disc measurements in myopia with optical coherence tomography and confocal scanning laser ophthalmoscopy. Invest. Opthalmol. Vis. Sci. 48 (7), 3178. http://dx.doi.org/10.1167/iovs.06-1315.

Leung, C.K., Lam, S., Weinreb, R.N., Liu, S., Ye, C., Liu, L., He, J., Lai, G.W., Li, T., Lam, D.S., 2010. Retinal nerve fiber layer imaging with spectral-domain optical coherence tomography. Ophthalmology 117 (9), 1684–1691. http://dx.doi.org/10.1016/j.ophtha.2010.01.026.

Leung, C.K.-S., Yu, M., Weinreb, R.N., Mak, H.K., Lai, G., Ye, C., Lam, D.S.-C., 2012. Retinal nerve fiber layer imaging with spectral-domain optical coherence tomography: Interpreting the RNFL maps in healthy myopic eyes. Invest. Opthalmol. Vis. Sci. 53 (11), 7194. http://dx.doi.org/10.1167/iovs.12-9726.

Li, J., Jin, P., Zhu, J., Zou, H., Xu, X., Tang, M., Zhou, M., Gan, Y., He, J., Ling, Y., Su, Y., 2021. Multi-scale GCN-assisted two-stage network for joint segmentation of retinal layers and discs in peripapillary OCT images. Biomed. Opt. Express 12 (4), 2204–2220. http://dx.doi.org/10.1364/BOE.417212.

Marcus, M.W., de Vries, M.M., Montolio, F.G.J., Jansonius, N.M., 2011. Myopia as a risk factor for open-angle glaucoma: A systematic review and meta-analysis. Ophthalmology 118 (10), 1989–1994.e2. http://dx.doi.org/10.1016/j.ophtha.2011.03.012.

Moriyama, M., Ohno-Matsui, K., Hayashi, K., Shimada, N., Yoshida, T., Tokoro, T., Morita, I., 2011. Topographic analyses of shape of eyes with pathologic myopia by high-resolution three-dimensional magnetic resonance imaging. Ophthalmology 118 (8), 1626–1637. http://dx.doi.org/10.1016/j.ophtha.2011.01.018.

Murphy, M.L., Pokrovskaya, O., Galligan, M., O'Brien, C., 2017. Corneal hysteresis in patients with glaucoma-like optic discs, ocular hypertension and glaucoma. BMC Ophthalmol. 17 (1), http://dx.doi.org/10.1186/s12886-016-0396-9.

Mwanza, J.-C., Budenz, D.L., 2016. Optical coherence tomography platforms and parameters for glaucoma diagnosis and progression. Curr. Opin. Ophthalmol. 27 (2), 102–110. http://dx.doi.org/10.1097/icu.0000000000000231.

Mwanza, J.-C., Durbin, M.K., Budenz, D.L., Sayyad, F.E., Chang, R.T., Neelakantan, A., Godfrey, D.G., Carter, R., Crandall, A.S., 2012. Glaucoma diagnostic accuracy of ganglion cell–Inner plexiform layer thickness: Comparison with nerve fiber layer and optic nerve head. Ophthalmology 119 (6), 1151–1158. http://dx.doi.org/10.1016/j.ophtha.2011.12.014.

Na, J.H., Sung, K.R., Baek, S., Sun, J.H., Lee, Y., 2011. Macular and retinal nerve fiber layer thickness: Which is more helpful in the diagnosis of glaucoma? Invest. Opthalmol. Vis. Sci. 52 (11), 8094. http://dx.doi.org/10.1167/iovs.11-7833.

Na, J.H., Sung, K.R., Lee, J.R., Lee, K.S., Baek, S., Kim, H.K., Sohn, Y.H., 2013. Detection of glaucomatous progression by spectral-domain optical coherence tomography. Ophthalmology 120 (7), 1388–1395. http://dx.doi.org/10.1016/j.ophtha.2012.12.014.

Nouri-Mahdavi, K., Nowroozizadeh, S., Nassiri, N., Cirineo, N., Knipping, S., Giaconi, J., Caprioli, J., 2013. Macular ganglion cell/inner plexiform layer measurements by spectral domain optical coherence tomography for detection of early glaucoma and comparison to retinal nerve fiber layer measurements. Am. J. Ophthalmol. 156 (6), 1297–1307.e2. http://dx.doi.org/10.1016/j.ajo.2013.08.001.

Paszke, A., Gross, S., Massa, F., Lerer, A., Bradbury, J., Chanan, G., Killeen, T., Lin, Z., Gimelshein, N., Antiga, L., Desmaison, A., Kopf, A., Yang, E., DeVito, Z., Raison, M., Tejani, A., Chilamkurthy, S., Steiner, B., Fang, L., Bai, J., Chintala, S., 2019. PyTorch: An imperative style, high-performance deep learning library. In: Advances in Neural Information Processing Systems, vol. 32. Curran Associates, Inc., pp. 8024–8035, URL http://papers.neurips.cc/paper/9015-pytorch-an-imperative-style-high-performance-deep-learning-library.pdf.

Rispoli, M., Cennamo, G., Antonio, L.D., Lupidi, M., Parravano, M., Pellegrini, M., Veritti, D., Vujosevic, S., Savastano, M.C., 2023. Practical guidance for imaging biomarkers in exudative age-related macular degeneration. Surv. Ophthalmol. 68 (4), 615–627. http://dx.doi.org/10.1016/j.survophthal.2023.02.004.

Roy, A.G., Conjeti, S., Karri, S.P.K., Sheet, D., Katouzian, A., Wachinger, C., Navab, N., 2017. ReLayNet: retinal layer and fluid segmentation of macular optical coherence tomography using fully convolutional networks. Biomed. Opt. Express 8 (8), 3627. http://dx.doi.org/10.1364/boe.8.003627.

Russakoff, D.B., Mannil, S.S., Oakley, J.D., Ran, A.R., Cheung, C.Y., Dasari, S., Riyazzuddin, M., Nagaraj, S., Rao, H.L., Chang, D., Chang, R.T., 2020. A 3D deep learning system for detecting referable glaucoma using full OCT macular cube scans. Transl. Vis. Sci. Technol. 9 (2), 12. http://dx.doi.org/10.1167/tvst.9.2.12.

Schlegl, T., Waldstein, S.M., Bogunovic, H., Endstraßer, F., Sadeghipour, A., Philip, A.-M., Podkowinski, D., Gerendas, B.S., Langs, G., Schmidt-Erfurth, U., 2018. Fully automated detection and quantification of macular fluid in OCT using deep learning. Ophthalmology 125 (4), 549–558. http://dx.doi.org/10.1016/j.ophtha.2017.10.031.

Shaikh, Y., Yu, F., Coleman, A.L., 2014. Burden of undetected and untreated glaucoma in the United States. Am. J. Ophthalmol. 158 (6), 1121–1129.e1. http://dx.doi.org/10.1016/j.ajo.2014.08.023.

Suwan, Y., Rettig, S., Park, S.C., Tantraworasin, A., Geyman, L.S., Effert, K., Silva, L., Jarukasetphorn, R., Ritch, R., 2018. Effects of circumpapillary retinal nerve fiber layer segmentation error correction on glaucoma diagnosis in myopic eyes. J. Glaucoma 27 (11), 971–975. http://dx.doi.org/10.1097/ijg.0000000000001054.

Tabernero, J., Schaeffel, F., 2009. More irregular eye shape in low myopia than in emmetropia. Invest. Opthalmol. Vis. Sci. 50 (9), 4516. http://dx.doi.org/10.1167/iovs.09-3441.

Tan, N.Y.Q., Sng, C.C.A., Jonas, J.B., Wong, T.Y., Jansonius, N.M., Ang, M., 2019. Glaucoma in myopia: diagnostic dilemmas. Br. J. Ophthalmol. 103 (10), 1347–1355. http://dx.doi.org/10.1136/bjophthalmol-2018-313530.

Vidal, P., de Moura, J., Novo, J., Ortega, M., 2023. Multivendor fully automatic uncertainty management approaches for the intuitive representation of DME fluid accumulations in OCT images. Med. Biol. Eng. Comput. 61 (5), 1209–1224. http://dx.doi.org/10.1007/s11517-022-02765-z.

Welch, B.L., 1947. The generalization of 'student's' problem when several different population varlances are involved. Biometrika 34 (1–2), 28–35. http://dx.doi.org/10.1093/biomet/34.1-2.28.

W.H. Organization, 2019. World report on vision. World Health Organization, p. 160.

Yamashita, T., Kii, Y., Tanaka, M., Yoshinaga, W., Yamashita, T., Nakao, K., Sakamoto, T., 2014. Relationship between supernormal sectors of retinal nerve fibre layer and axial length in normal eyes. Acta Ophthalmol. 92 (6), http://dx.doi.org/10.1111/aos.12382.